Supplementary information for

Mitochondrial Rewiring with Small-Molecule Drug-Free Nanoassemblies Unleashes Anticancer Immunity

Authors: Lulu Ren,[1,2] Jianqin Wan,[1] Xiaoyan Li,[1,3] Jie Yao,[1,3] Yan Ma,[1] Fanchao Meng,[1] Shusen Zheng,[1]* Weidong Han,[4]* and Hangxiang Wang [1,2,5]*

Affiliations: [1]*The First Affiliated Hospital, NHC Key Laboratory of Combined Multi-Organ Transplantation, Collaborative Innovation Center for Diagnosis and Treatment of Infectious Diseases, State Key Laboratory for Diagnosis and Treatment of Infectious Diseases, Zhejiang University School of Medicine, Hangzhou, Zhejiang Province 310003, P. R. China.* [2]*Jinan Microecological Biomedicine Shandong Laboratory, Jinan, Shandong Province 250117, P. R. China.* [3]*Department of Chemical Engineering, Zhejiang University, Hangzhou, Zhejiang Province 310027, P.R. China.* [4]*Department of Colorectal Medical Oncology, Zhejiang Cancer Hospital, Hangzhou, Zhejiang Province 310022, P. R. China.* [5]*Department of Hepatobiliary Surgery, The First Affiliated Hospital, Wenzhou Medical University, Wenzhou, Zhejiang Province, 325000, P. R. China.*

*Corresponding author. Email: wanghx@zju.edu.cn (H. W.); hanwd@zjcc.org.cn (W.H.); shusenzheng@zju.edu.cn (S. Z.).
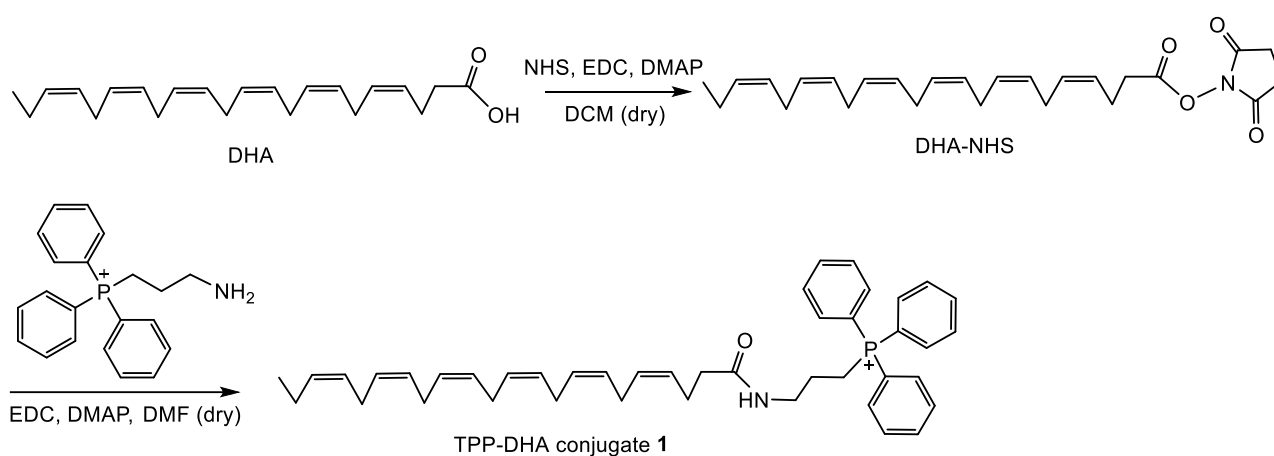
The PDF file includes:

Supplementary Methods

Supplementary Figures 1 to 32

Supplementary Tables 1 to 2

Supplementary Methods

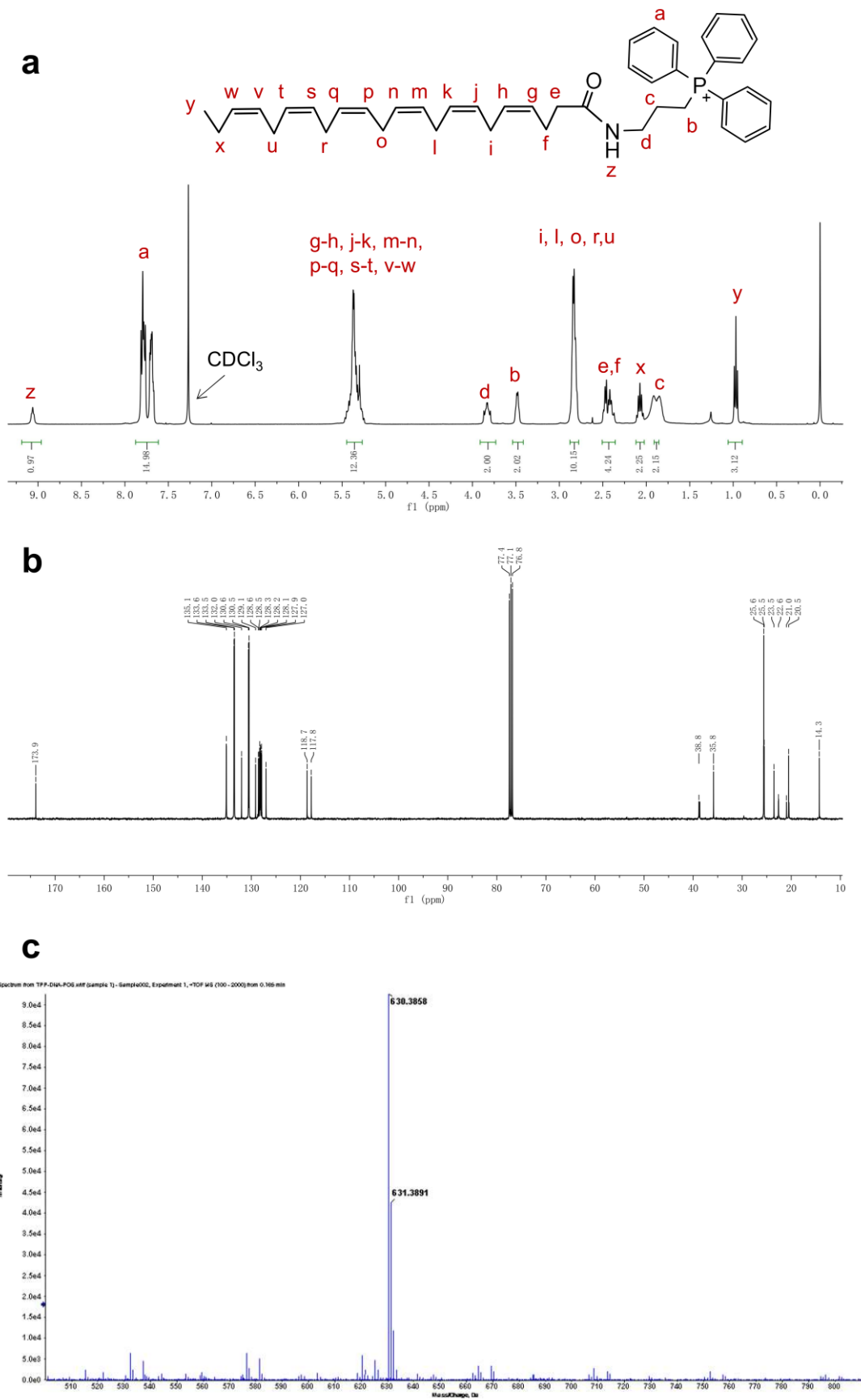### Synthesis of TPP-DHA conjugate 1

DHA (147.8 mg, 0.45 mmol) was first activated by *N*-hydroxysuccinimide (NHS). To a solution of TPP (200.2 mg, 0.50 mmol) and DHA-NHS in 4 mL of anhydrous N,N-Dimethylformamide (DMF) were added 1-ethyl-3-(3-dimethylaminopropyl) carbodiimide (EDC, 77.6 mg, 0.50 mmol) and 4-dimethylamino pyridine (DMAP, 61.1 mg, 0.50 mmol). The reaction mixture was stirred at 45°C for 8 h. After removing the solvent, dichloromethane (DCM) was added and washed with 5% aqueous citric acid, saturated NaHCO$_3$ solution and brine. The organic layer was dried over anhydrous Na$_2$SO$_4$, filtered, and evaporated under vacuum. The residue was purified by flash column chromatography on silica gel (DCM:MeOH=20:1) to give TPP-DHA conjugate **1** (135.9 mg, 42.5%).

^{1}H NMR (400 MHz, CDCl$_3$) δ 9.07-9.05 (t, *J* = 4 Hz, 1H), 7.81-7.67 (m, 15H), 5.47-5.25 (m, 12H), 3.87-3.79 (dd, *J* = 16, 12 Hz, 2H), 3.49-3.48 (d, *J* = 4 Hz, 2H), 2.84-2.82 (m, 10H), 2.49-2.37 (m, 4H), 2.11-2.04 (m, 2H), 1.86 (s, 2H), 0.99-0.95 (t, *J* = 8 Hz, 3H).

^{13}C NMR (100 MHz, CDCl$_3$) δ 173.9, 135.1, 135.1, 135.1, 133.6, 133.6, 133.6, 133.5, 133.5, 133.5, 132.0, 130.6, 130.6, 130.6, 130.5, 130.5, 130.5, 129.1, 128.6, 128.5, 128.3, 128.2, 128.2, 128.1, 127.9, 127.9, 127.0, 127.0, 118.7, 117.8, 117.8, 38.8, 35.8, 25.6, 25.6, 25.6, 25.5, 23.5, 22.6, 21.0, 20.5, 20.5, 14.3.

HRMS: calcd for [C$_{43}$H$_{53}$NOP]$^+$ = 630.3859; obsd: 630.3858.

Supplementary Figure 1. a, ^{1}H NMR spectrum of TPP-DHA conjugate **1** in CDCl$_3$. **b**, ^{13}C NMR spectrum of TPP-DHA conjugate **1** in CDCl$_3$. **c**, High-resolution mass spectrum of TPP-DHA conjugate **1**.
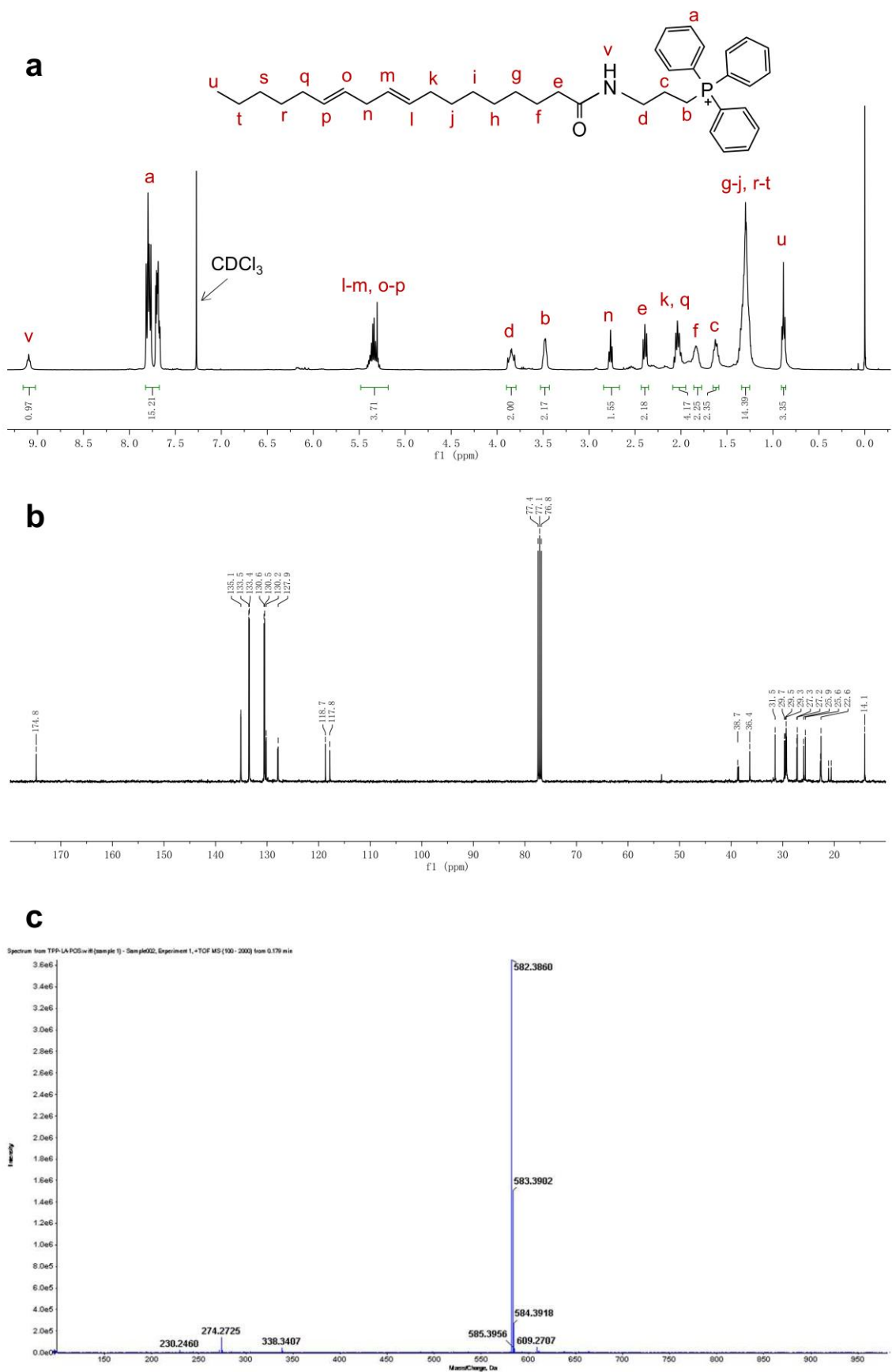
S3

Synthesis of TPP-LA conjugate 2
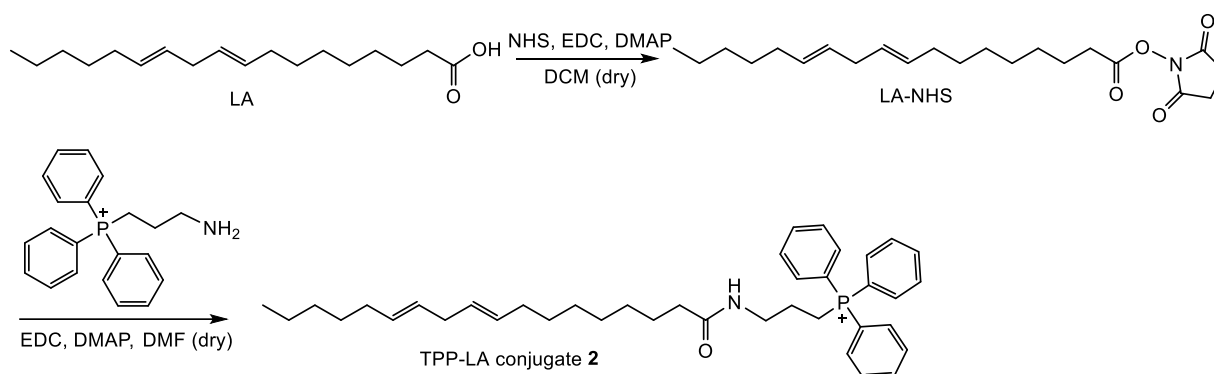
LA (126.2 mg, 0.45 mmol) was first activated by NHS. To a solution of TPP (200.2 mg, 0.50 mmol) and LA-NHS in 4 mL of anhydrous DMF were added EDC (77.6 mg, 0.50 mmol) and DMAP (61.1 mg, 0.50 mmol). The reaction mixture was stirred at 45 ℃ for 8 hours. After removing the solvent, dichloromethane was added and washed with 5% aqueous citric acid, saturated NaHCO$_3$ solution and brine. The organic layer was dried over anhydrous Na$_2$SO$_4$, filtered, and evaporated under vacuum. The residue was purified by flash column chromatography on silica gel (DCM:MeOH=20:1) to give TPP-LA conjugate **2** (145.8 mg, 48.9%).

^{1}H NMR (400 MHz, CDCl$_3$) δ 9.11-9.08 (t, J = 6 Hz, 1H), 7.82-7.61 (m, 15H), 5.41-5.28 (m, 4H), 3.88-3.81 (dd, J = 16, 12 Hz, 2H), 3.49-3.47 (m, 2H), 2.78-2.75 (t, J = 6 Hz, 2H), 2.41-2.37 (t, J =8 Hz, 2H), 2.07-2.00 (m, 4H), 1.88-1.79 (m, 2H), 1.64-1.59 (m, 2H), 1.39-1.22 (m, 14H), 0.90-0.87 (t, J = 6 Hz, 3H).

^{13}C NMR (100 MHz, CDCl$_3$) δ 174.8, 135.1, 135.1, 135.1, 133.5, 133.5, 133.5, 133.4, 133.4, 133.4, 130.6, 130.6, 130.6, 130.5, 130.5, 130.5, 130.2, 130.2, 127.9, 127.9, 118.7, 117.8, 117.8, 38.7, 36.4, 31.5, 29.7, 29.5, 29.4, 29.3, 27.3, 27.2, 25.9, 25.6, 22.7, 22.6, 21.1, 20.6, 14.1.

HRMS: calcd for [C$_{39}$H$_{53}$NOP]$^+$ = 582.3859; obsd: 582.3860.

Supplementary Figure 2. a, ^{1}H NMR spectrum of TPP-LA conjugate **2** in CDCl$_3$. **b**, ^{13}C NMR spectrum of TPP-LA conjugate **2** in CDCl$_3$. **c**, High-resolution mass spectrum of TPP-LA conjugate **2**.
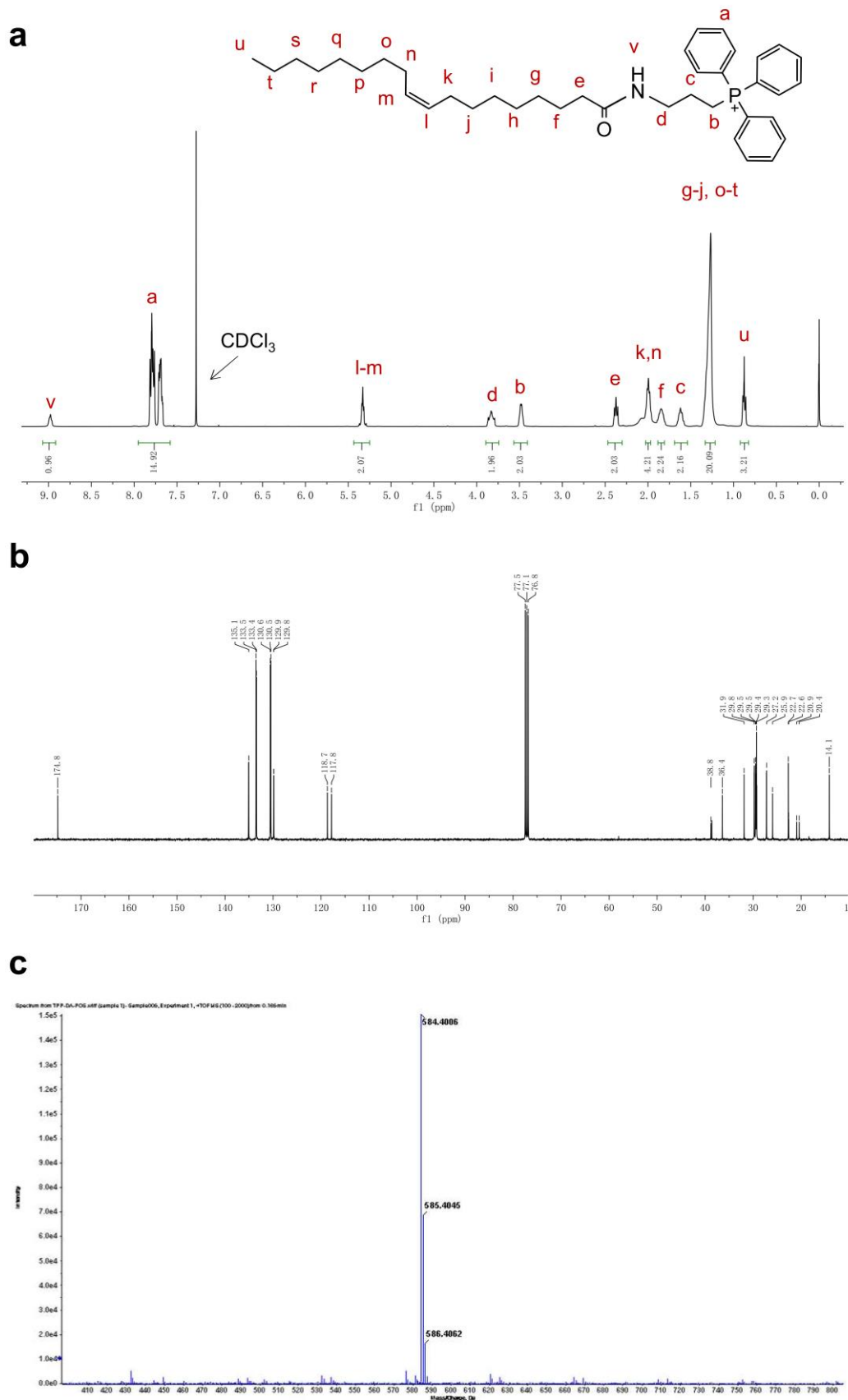
Synthesis of mtDSN-3
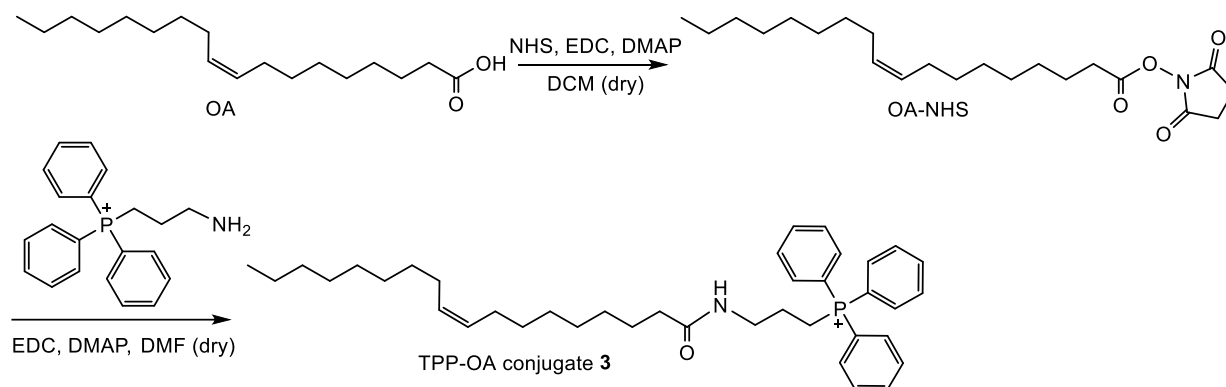
OA (127.1 mg, 0.45 mmol) was first activated by NHS. To a solution of TPP (200.2 mg, 0.50 mmol) and OA-NHS in 4 mL of anhydrous DMF were added EDC (77.6 mg, 0.50 mmol) and DMAP (61.1 mg, 0.50 mmol). The reaction mixture was stirred at 45 ℃ for 8 hours. After removing the solvent, dichloromethane was added and washed with 5% aqueous citric acid, saturated NaHCO$_3$ solution and brine. The organic layer was dried over anhydrous Na$_2$SO$_4$, filtered, and evaporated under vacuum. The residue was purified by flash column chromatography on silica gel (DCM:MeOH=20:1) to give TPP-OA conjugate **3** (101.4 mg, 33.9%).

^{1}H NMR (400 MHz, CDCl$_3$) δ 8.99-8.96 (t, J = 6 Hz, 1H), 7.81-7.67 (m, 15H), 5.37-5.29 (m, 2H), 3.86-3.79(m, 2H), 3.48 (s, 2H), 2.39-2.35 (t, J = 8 Hz, 2H), 2.01-1.98 (t, J = 6 Hz, 4H), 1.85 (s, 2H), 1.62-1.60 (m, 2H), 1.27 (s, 20H), 0.89-0.86 (t, J = 6 Hz, 3H).

^{13}C NMR (100 MHz, CDCl$_3$) δ 174.8, 135.1, 135.1 135.1, 133.5, 133.5, 133.5, 133.4, 133.4, 133.4, 130.6, 130.6, 130.6, 130.5, 130.5, 130.5, 129.9, 129.8, 118.7, 117.8, 117.8, 38.8, 36.4, 31.9, 29.8, 29.8, 29.5, 29.5, 29.5, 29.4, 29.3, 27.2, 25.9, 22.7, 22.7, 22.6, 20.9, 20.4, 14.1.

HRMS: calcd for [C$_{39}$H$_{55}$NOP]$^+$ = 584.4016; obsd: 584.4006.

Supplementary Figure 3. a, ¹H NMR spectrum of TPP-OA conjugate **3** in CDCl₃. **b**, ¹³C NMR spectrum of TPP-OA conjugate **3** in CDCl₃. **c**, High-resolution mass spectrum of TPP-OA conjugate **3**.
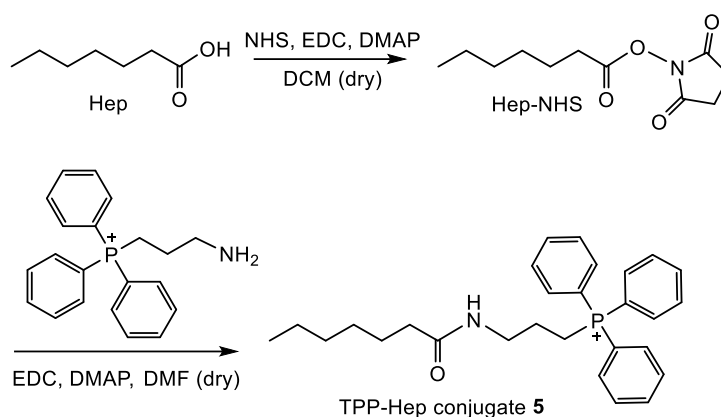
Synthesis of mtDSN-4
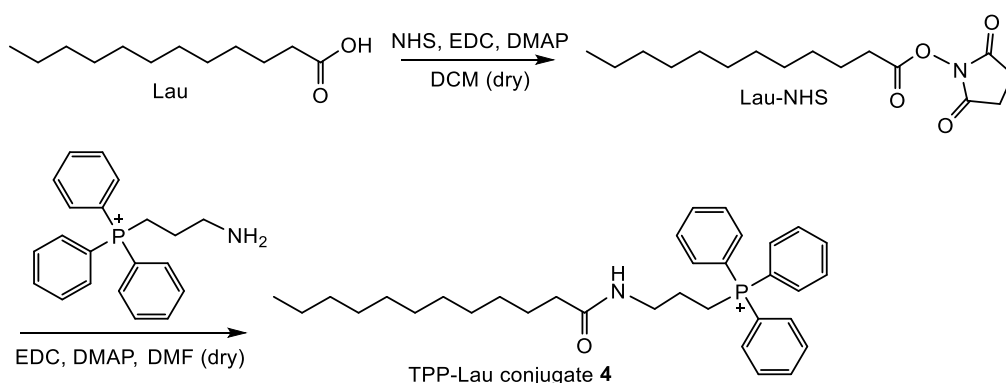
Lau (90.1 mg, 0.45 mmol) was first activated by NHS. To a solution of TPP (200.2 mg, 0.50 mmol) and Lau-NHS in 4 mL of anhydrous DMF were added EDC (77.6 mg, 0.50 mmol) and DMAP (61.1 mg, 0.50 mmol). The reaction mixture was stirred at 45 ℃ for 8 hours. After removing the solvent, dichloromethane was added and washed with 5% aqueous citric acid, saturated $NaHCO_3$ solution and brine. The organic layer was dried over anhydrous Na_2SO_4, filtered, and evaporated under vacuum. The residue was purified by flash column chromatography on silica gel (DCM:MeOH=20:1) to give TPP-Lau conjugate **4** (105.6 mg, 40.3%).

^{1}H NMR (400 MHz, CDCl$_3$) δ 9.01-8.98 (t, J = 6 Hz, 1H), 7.82-7.67 (m, 15H), 3.88-3.81 (m, 2H), 3.50-3.47 (m, 2H), 2.40-2.36 (t, J = 8 Hz, 2H), 1.87-1.82 (m, 2H), 1.65-1.58 (m, 2H), 1.31-1.19(m, 16H), 0.89-0.86 (t, J = 6 Hz, 3H).

^{13}C NMR (100 MHz, CDCl$_3$) δ 174.8, 135.1, 135.1, 135.1, 133.5, 133.5, 133.5, 133.4, 133.4, 133.4, 130.6, 130.6, 130.6, 130.5, 130.5, 130.5, 118.7, 117.8, 117.8, 38.7, 36.4, 31.9, 29.6, 29.6, 29.6, 29.4, 29.3, 26.0, 22.7, 22.6, 21.0, 20.5, 14.1.

HRMS: calcd for [C$_{33}$H$_{45}$NOP]$^+$ = 502.3233; obsd: 502.3227.

Supplementary Figure 4. a, ^{1}H NMR spectrum of TPP-Lau conjugate **4** in CDCl$_3$. **b**, ^{13}C NMR spectrum of TPP-Lau conjugate **4** in CDCl$_3$. **c**, High-resolution mass spectrum of TPP-Lau conjugate **4**.

Synthesis of mtDSN-5

Hep (58.6 mg, 0.45 mmol) was first activated by NHS. To a solution of TPP (200.2 mg, 0.50 mmol) and Hep-NHS in 4 mL of anhydrous DMF were added EDC (77.6 mg, 0.50 mmol) and DMAP (61.1 mg, 0.50 mmol). The reaction mixture was stirred at 45 ℃ for 8 h. After removing the solvent, dichloromethane was added and washed with 5% aqueous citric acid, saturated $NaHCO_3$ solution and brine. The organic layer was dried over anhydrous Na_2SO_4, filtered, and evaporated under vacuum. The residue was purified by flash column chromatography on silica gel (DCM:MeOH=20:1) to give TPP-Hep conjugate **5** (110.5 mg, 47.9%).

^{1}H NMR (400 MHz, CDCl$_3$) δ 9.04-9.01 (t, J = 6 Hz, 1H), 7.82-7.67 (m, 15H), 3.87-3.80 (m, 2H), 3.50-3.46 (m, 2H), 2.40-2.36 (t, J = 8 Hz, 2H), 1.89-1.83 (m, 2H), 1.66-1.59 (m, 2H), 1.36-1.24 (m, 6H), 0.87-0.84 (t, J = 6 Hz, 3H).

^{13}C NMR (100 MHz, CDCl$_3$) δ 174.8, 135.1, 135.1, 135.1, 133.5, 133.5, 133.5, 133.4, 133.4, 133.4, 130.6, 130.6, 130.6, 130.5, 130.5, 130.5, 118.6, 117.8, 117.8, 38.7, 36.4, 31.7, 29.1, 25.9, 22.5, 21.1, 20.6, 14.1.
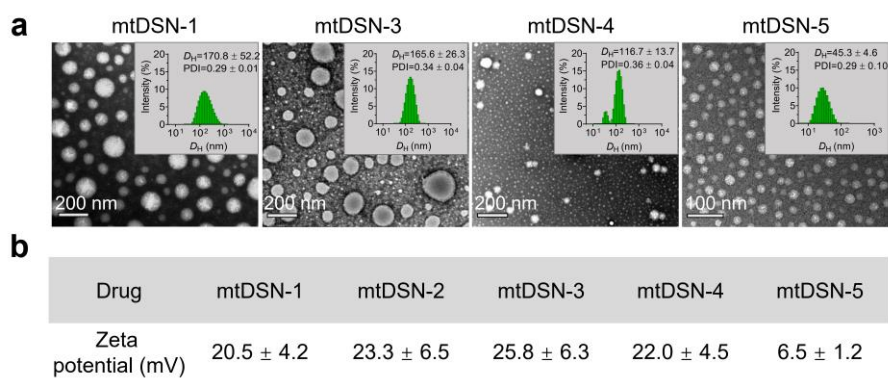
HRMS: calcd for $[C_{28}H_{35}NOP]^+$ = 432.2451; obsd: 432.2442.
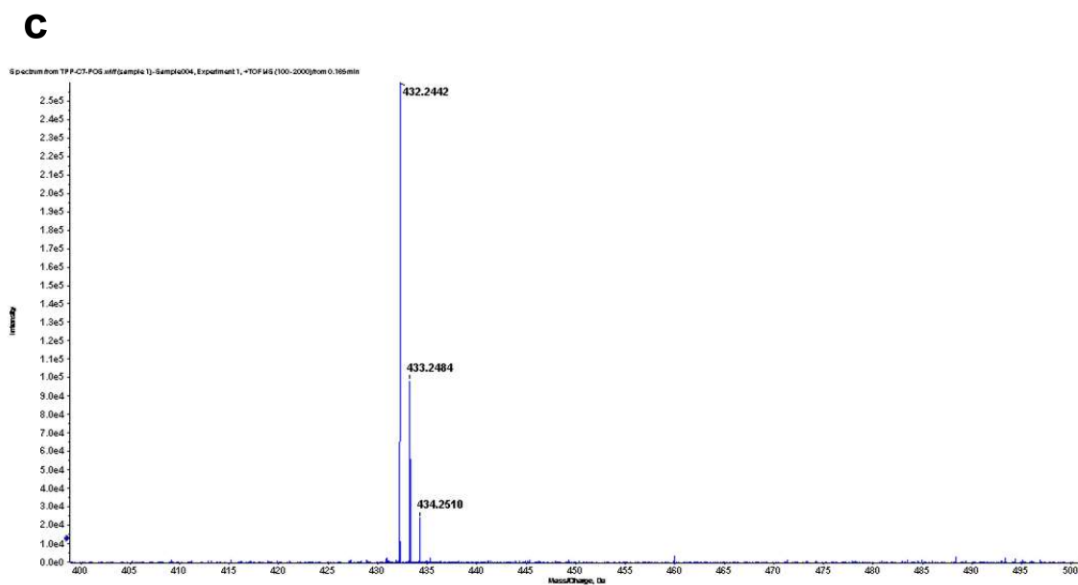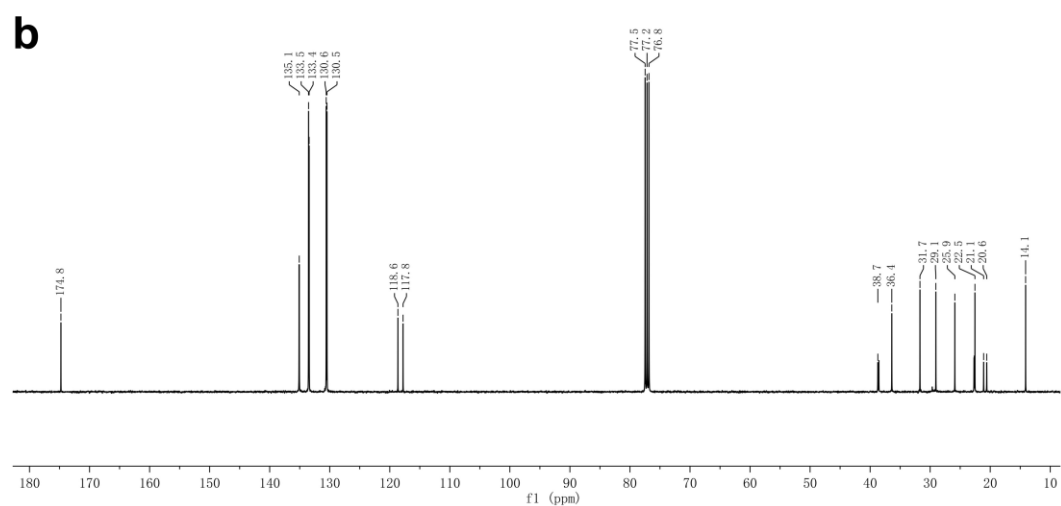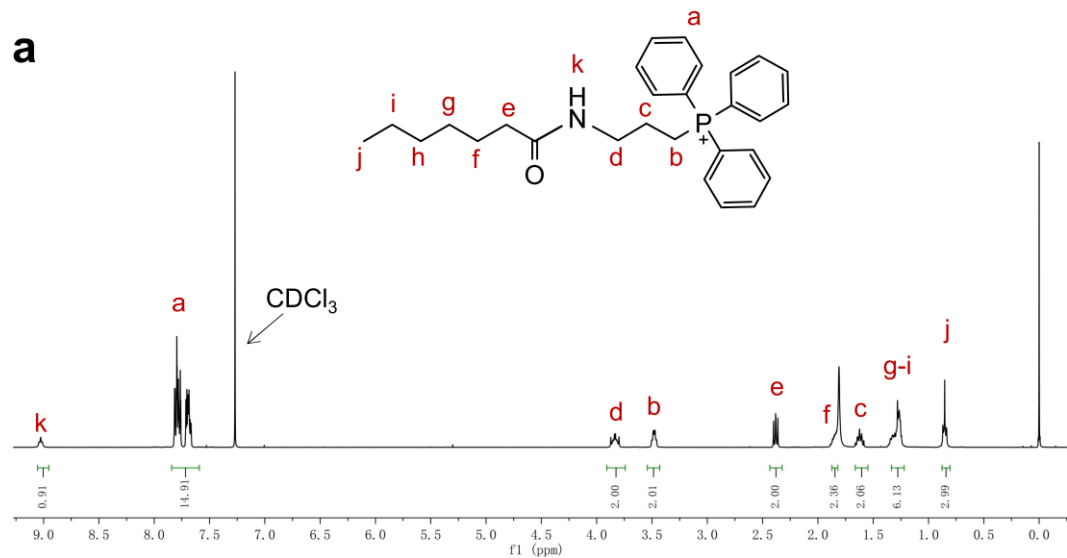
Supplementary Figure 5. a, ^{1}H NMR spectrum of TPP-Hep conjugate **5** in CDCl$_3$. **b**, ^{13}C NMR spectrum of TPP-Hep conjugate **5** in CDCl$_3$. **c**, High-resolution mass spectrum of TPP-Hep conjugate **5**.
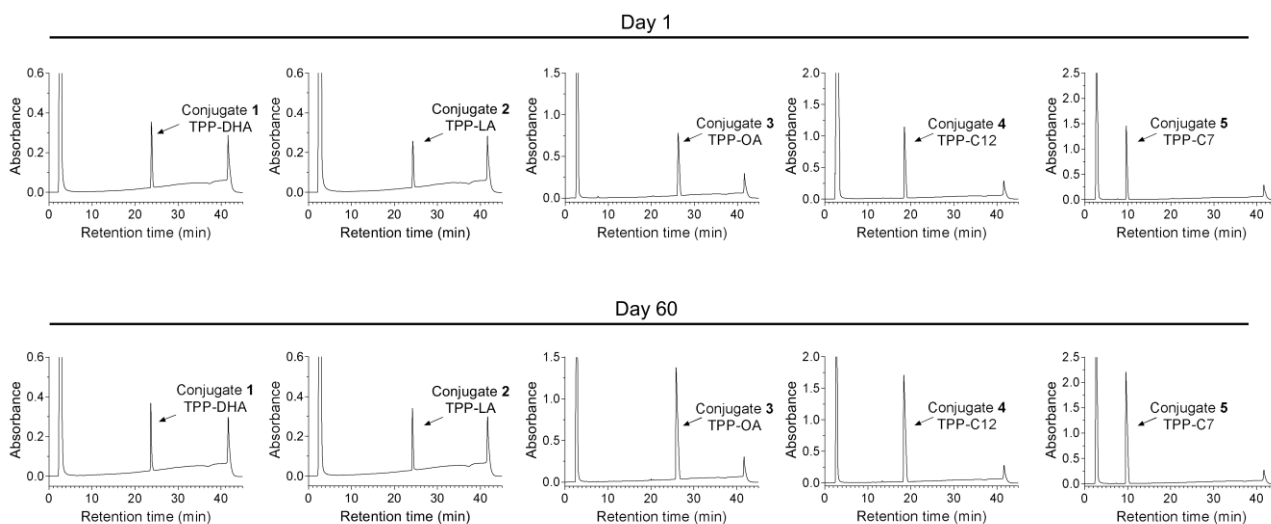
Supplementary Figure 6. High-performance liquid chromatography (HPLC) analysis of conjugates **1**–**5** on day 1 and day 60.

a

mtDSN-1	mtDSN-3	mtDSN-4	mtDSN-5
D_H=170.8 ± 52.2, PDI=0.29 ± 0.01	D_H=165.6 ± 26.3, PDI=0.34 ± 0.04	D_H=116.7 ± 13.7, PDI=0.36 ± 0.04	D_H=45.3 ± 4.6, PDI=0.29 ± 0.10
200 nm	200 nm	200 nm	100 nm

b

Drug	mtDSN-1	mtDSN-2	mtDSN-3	mtDSN-4	mtDSN-5
Zeta potential (mV)	20.5 ± 4.2	23.3 ± 6.5	25.8 ± 6.3	22.0 ± 4.5	6.5 ± 1.2

Supplementary Figure 7. a, TEM and size distribution characterization of mtDSN. D_H, hydrodynamic diameters. PDI, polydispersity index. **b**, Zeta potential measurement. All data are presented as the mean ± s.d. The results were shown from three biologically independent samples.
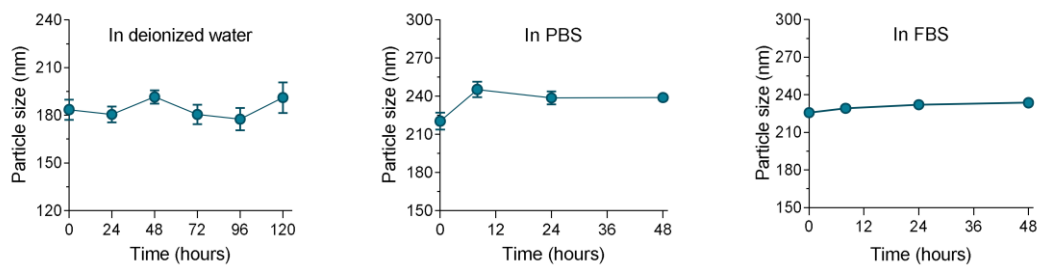
Supplementary Figure 8. Stability of mtDSN-2 in deionized water, PBS and PBS containing 10% FBS tested using DLS analysis. All data are presented as the mean ± s.d. The results were shown from three biologically independent samples. Source data are provided as a Source data file.
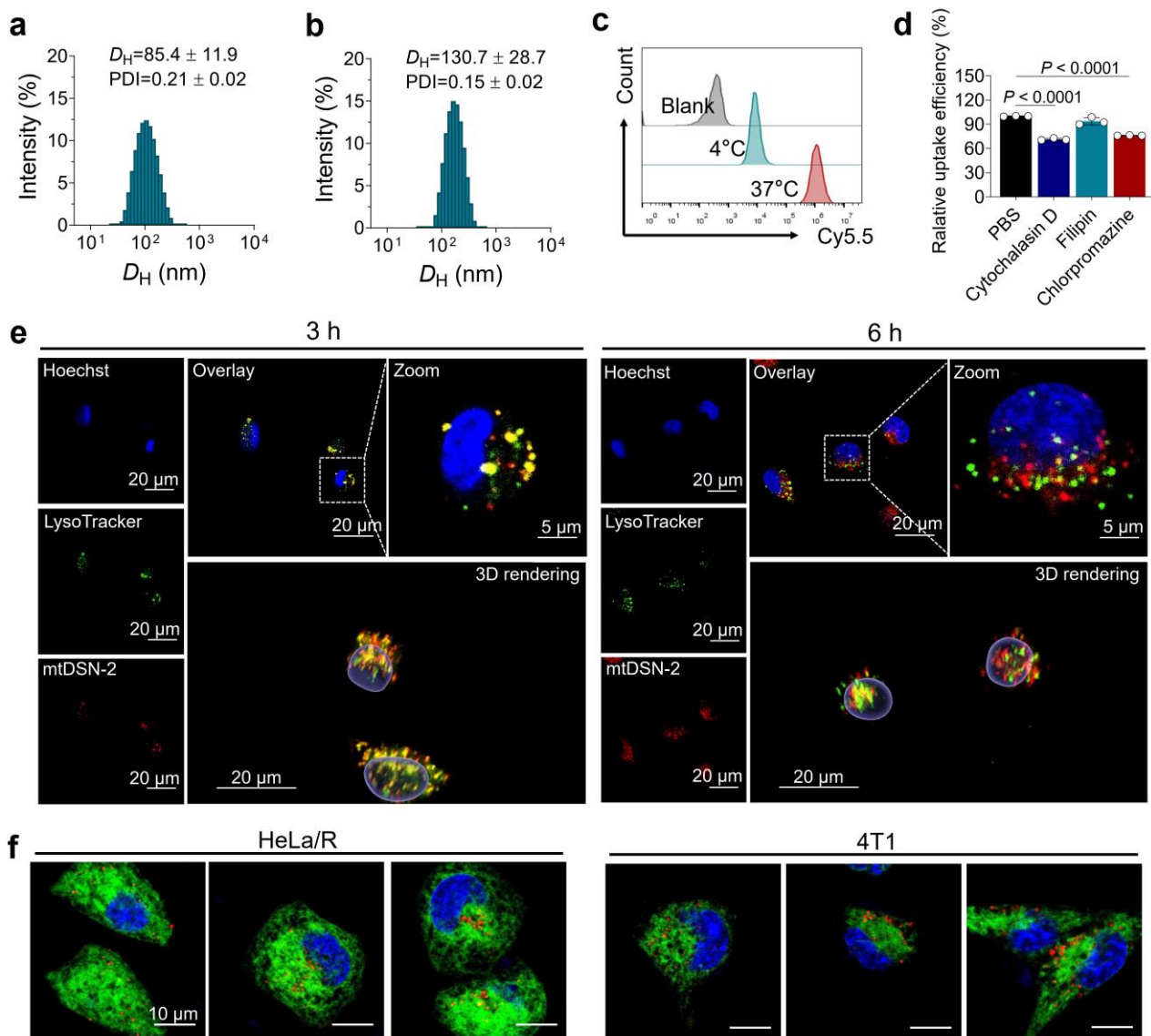
Supplementary Figure 9. a, Size distribution of nanoparticles self-assembled by Cy5.5-LA. **b**, Size distribution of Cy5.5-labeled mtDSN-2. **c**, Flow cytometry analysis of the cellular uptake of mtDSN-2 at 37 and 4°C. **d**, Examination of cellular uptake of mtDSN-2 upon pretreatment with inhibitors of specific endocytosis pathways. cytochalasin D (40 μM), filipin (5 μg/mL), and chlorpromazine (10 μg/mL) were used to block macropinocytosis, caveolin-mediated endocytosis, and clathrin-mediated endocytosis, respectively. **e**, Confocal microscopy images showing the colocalization of mtDSN-2 with lysosomes. Lysosome: LysoTracker Red DND-99 (green), mtDSN-2: Cy5.5 label (red), nuclei: Hoechst 33342 (blue). **f**, Confocal microscopy images showing the colocalization of mtDSN-2 with ER. ER: ER Tracker Green (green); mtDSN-2: Cy5.5 label (red), nuclei: Hoechst 33342 (blue). The data are presented as the mean ± s.d. The results were shown from three biologically independent samples. Statistical analysis by one-way ANOVA with Turkey's multiple comparisons test (**d**). Source data are provided as a Source data file.
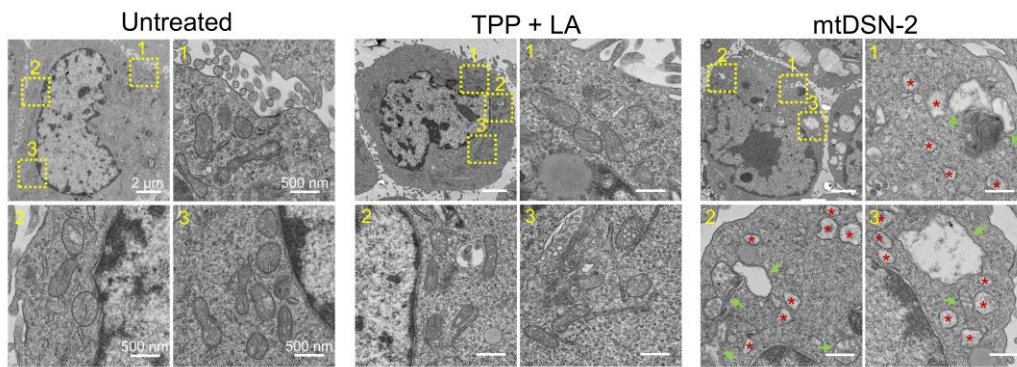
Supplementary Figure 10. TEM images of mitochondrial ultrastructure in 4T1 cancer cells following various treatments. Green arrows point to damaged mitochondria, while red asterisks mark areas of swelling endoplasmic reticulum. These images represent findings from three biologically independent experiments.
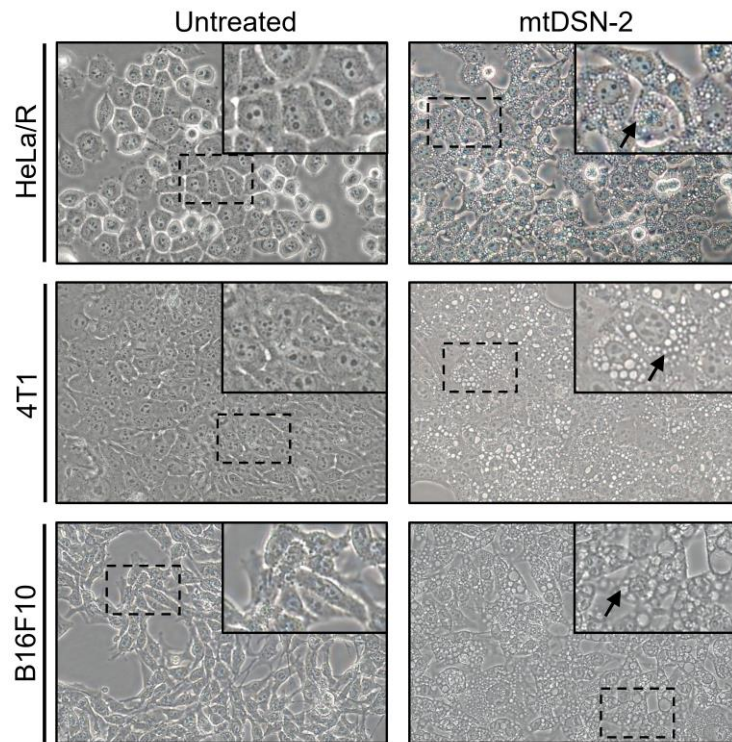
Supplementary Figure 11. Representative morphology of different tumor cells showing extensive cytoplasmic vacuolization (black arrows) upon exposure to mtDSN-2 (5 μM, 24 h). The results were shown from three biologically independent samples.
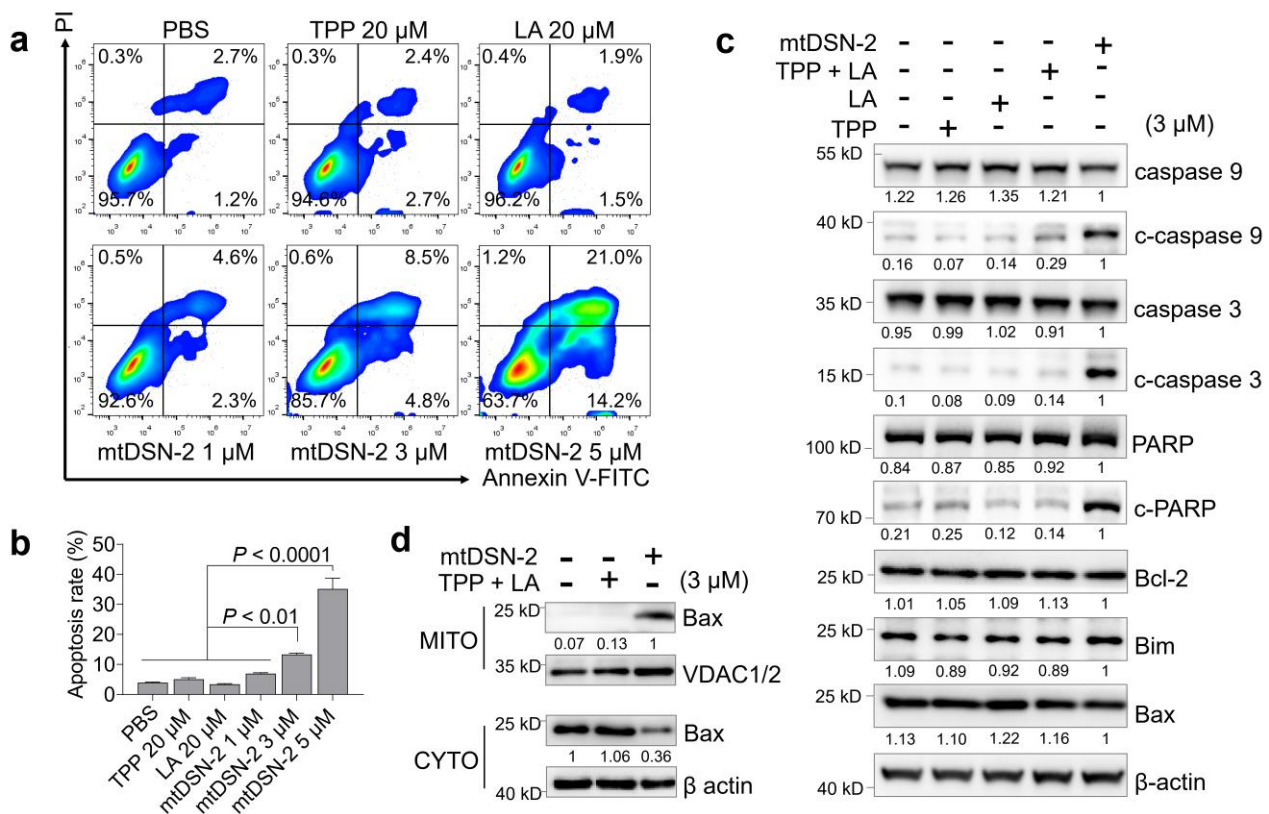
Supplementary Figure 12. a and **b**, Cell apoptosis was analyzed using Annexin-V/PI dual-staining. Tumor cells were treated as indicated for 48 h, and then submitted to flow cytometry for apoptosis rate quantification (n = 3). **c**, mtDSN-2 caused mitochondrial apoptosis, as evidenced by the formation of cleaved caspase 9, caspase 3, and PARP in cancer cells. **d**, Translocation of Bax from cytosol (CYTO) to mitochondria (MITO) after mtDSN-2 treatment. Band intensities were quantified from the 8-bit digital image by densitometry in ImageJ and are shown normalized for each target. The similar results were repeated in two biologically independent experiments (**c** and **d**). Statistical analysis by one-way ANOVA with Turkey's multiple comparisons test (**b**). Source data are provided as a Source data file.
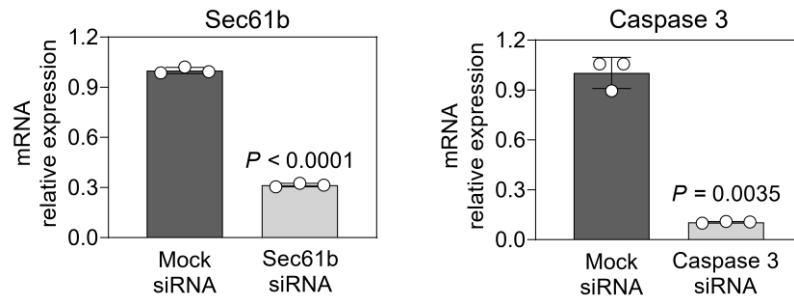
Supplementary Figure 13. Relative mRNA expression in 4T1 cells transfected with mock (untargeted), Sec61b or caspase 3 siRNA. The data are presented as the mean ± s.d. The results were shown from three biologically independent samples. Statistical analysis by Student's t test. Source data are provided as a Source data file.
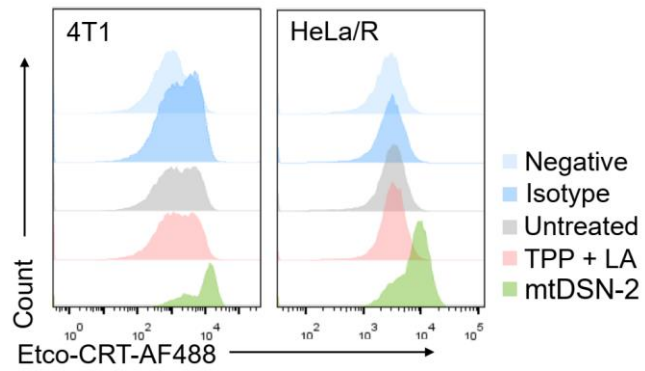
Supplementary Figure 14. The CRT exposure to cell surface was examined by immunofluorescence cytometry among viable cells (propidium iodine-negative). Negative: cells were not stained with antibodies. Isotype: cells were stained with isotype control antibodies. The results were shown from three biologically independent samples.
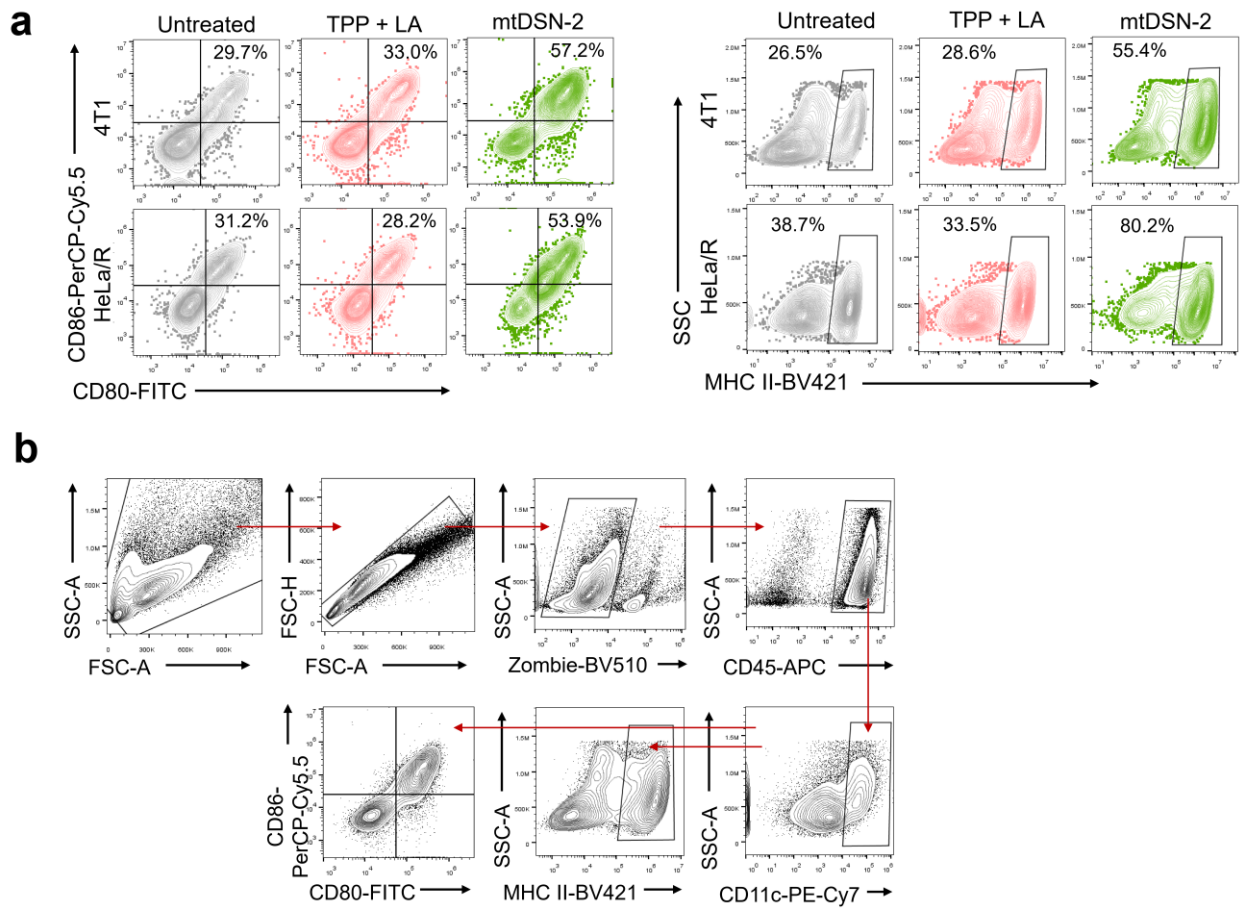
Supplementary Figure 15. a, Flow cytometry analysis of BMDCs maturation after exposure to culture media from different pretreated tumor cells for 24 h (gated as CD45$^+$CD11c$^+$ DCs). **b**, Gating scheme for **a**.
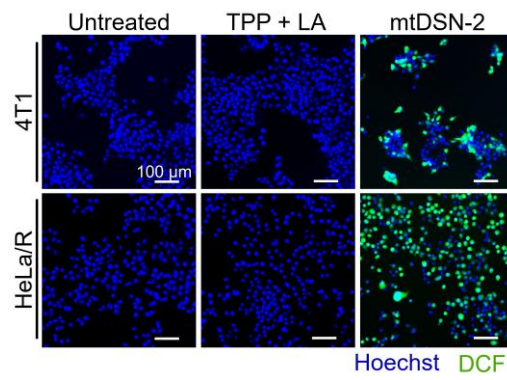
Supplementary Figure 16. Confocal microscopy analysis of intracellular ROS production by mtDSN-2 (5 μM, 24 h) using the fluorescent indicator DCFH-DA. The results were shown from three biologically independent samples.
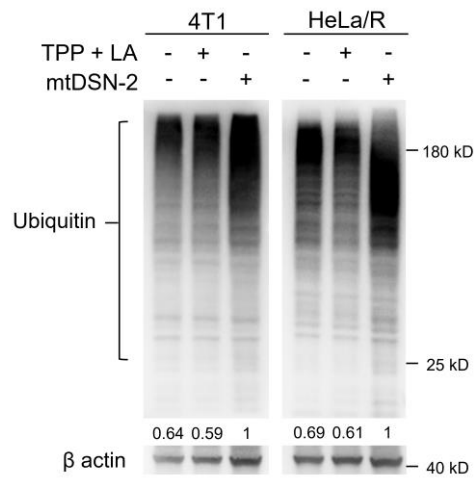
Supplementary Figure 17. Western blot analysis of ubiquitinated proteins after treatment (5 µM for 36 h). Band intensities were quantified from the 8-bit digital image by densitometry in ImageJ and are shown normalized to the mtDSN-2 lane. The similar results were repeated in two biologically independent experiments. Source data are provided as a Source data file.
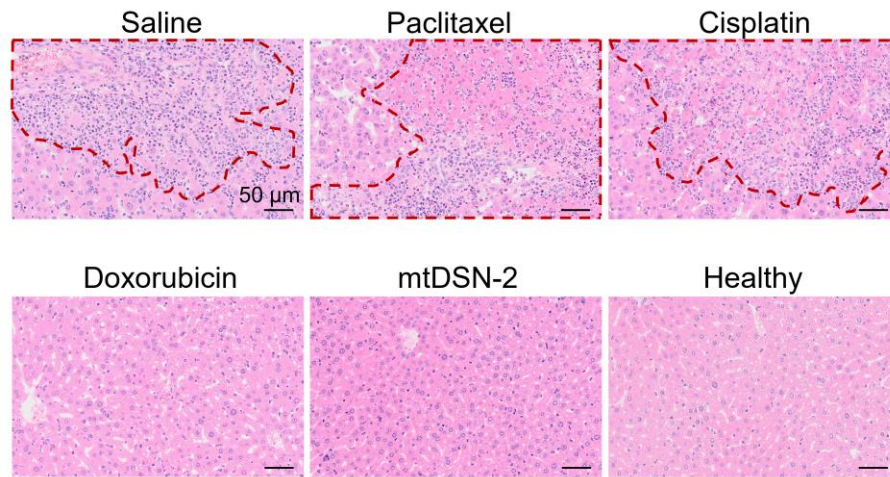
Supplementary Figure 18. Hematoxylin and eosin (H&E) staining analysis of tumor metastases (red dotted regions) to livers excised from each group. The similar results were obtained from three biologically independent samples.
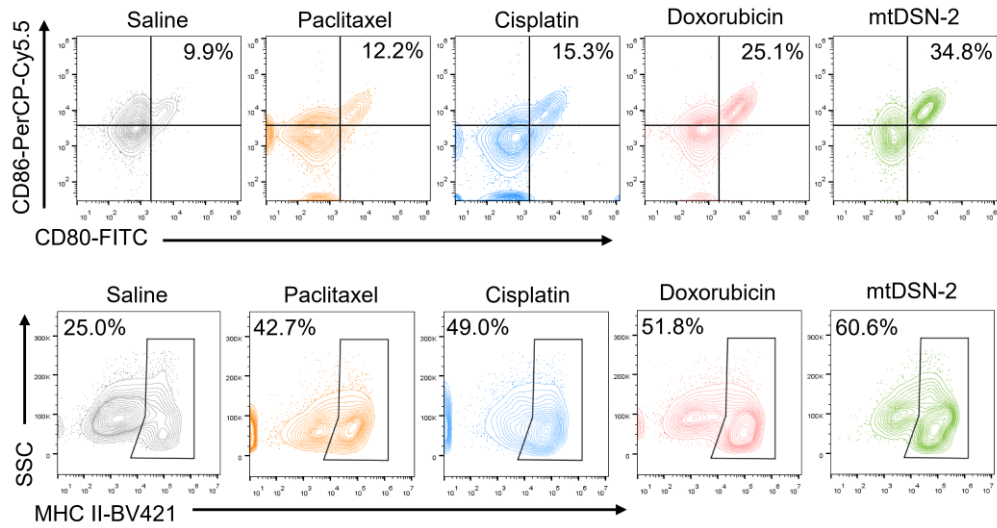
Supplementary Figure 19. Representative flow cytometric plots of DC maturation (gated as CD45$^+$CD11c$^+$ DCs) in the tumor-draining lymph nodes.
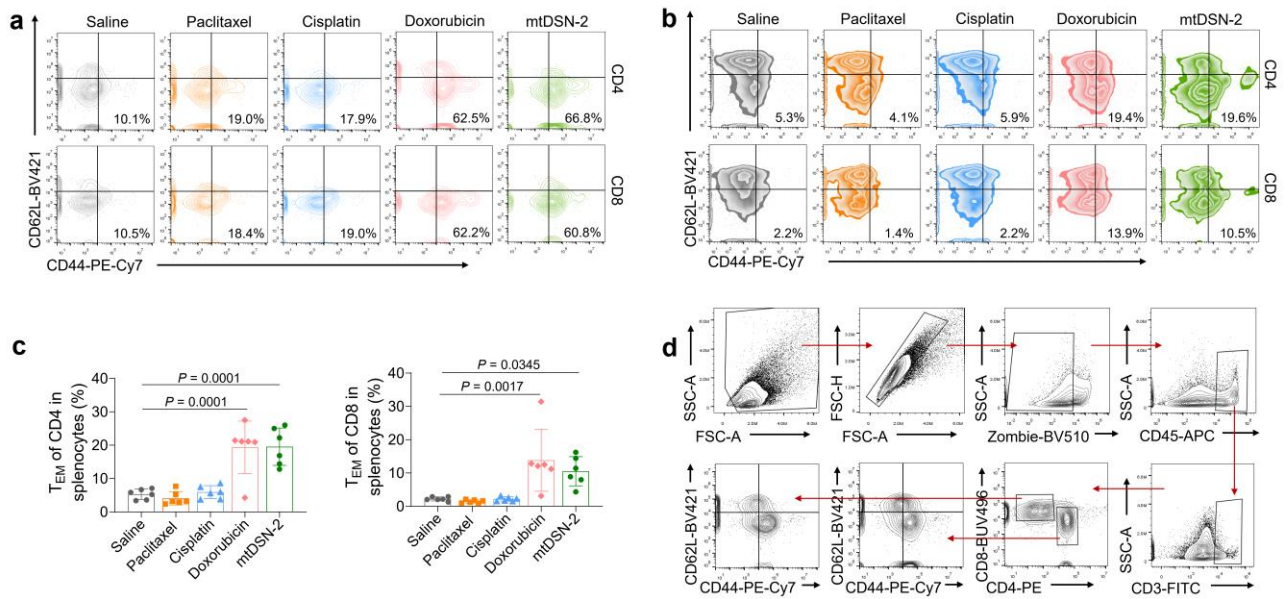
Supplementary Figure 20. a, Representative flow cytometric plots of effector memory T cells (T_{EM} gated as CD45^{+}CD3^{+}CD4/CD8^{+} T cells) in the orthotopic 4T1 tumors. **b** and **c**, Flow cytometric plots (**b**) and quantification (**c**) of T_{EM} in spleens (n = 6 mice/group). **d**, Gating scheme for flow cytometric analysis of T_{EM}. The data are presented as the mean ± s.d. Statistical analysis by one-way ANOVA with Turkey's multiple comparisons test (**c**). Source data are provided as a Source data file.
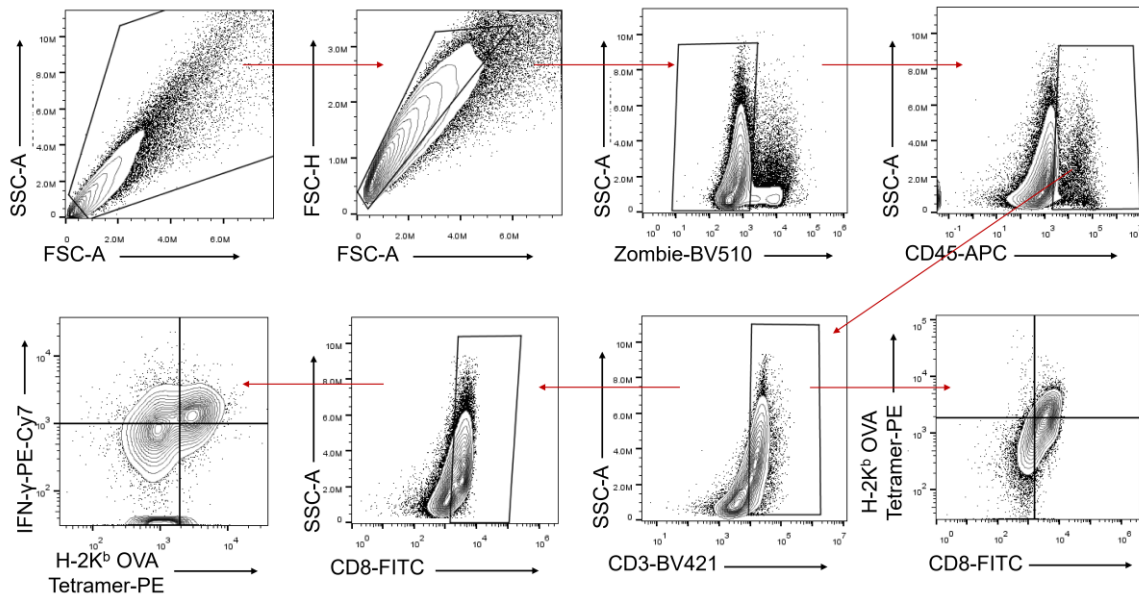
Supplementary Figure 21. Flow cytometry gating strategy for activated H-2K^b-restricted OVA$_{257-264}$-specific CD8$^+$ T cells.
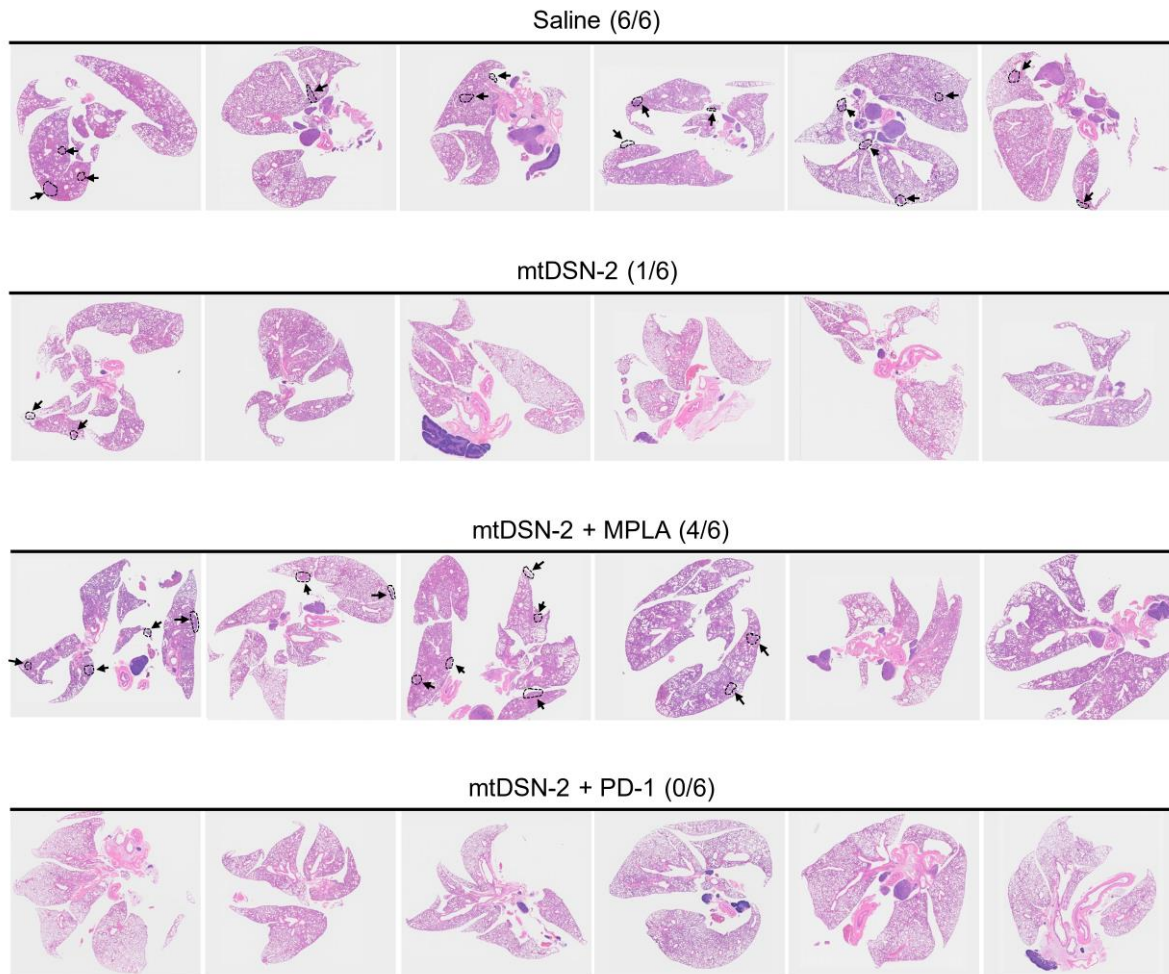
Supplementary Figure 22. H&E staining analysis of tumor metastases (black dotted circles) to lungs in each group (n = 6 mice/group).
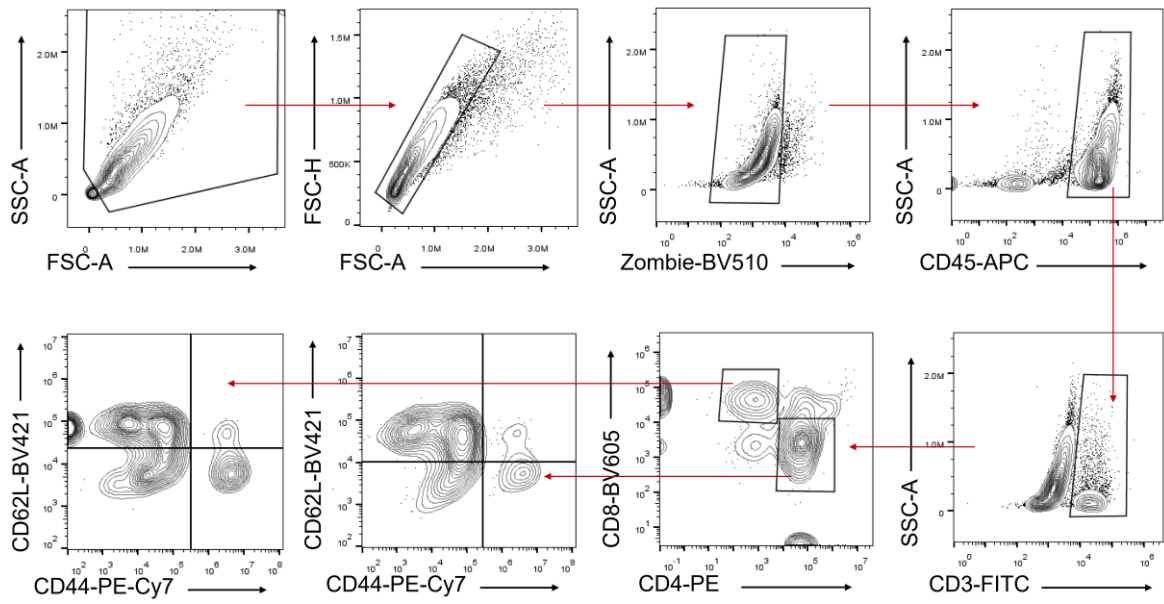
Supplementary Figure 23. Flow cytometry gating strategy for memory T cells.

MC38 (S0) MC38 (S3)

mtDSN-2-treated MC38 (S3)

50 µm

DAPI F4/80 CD86 CD206
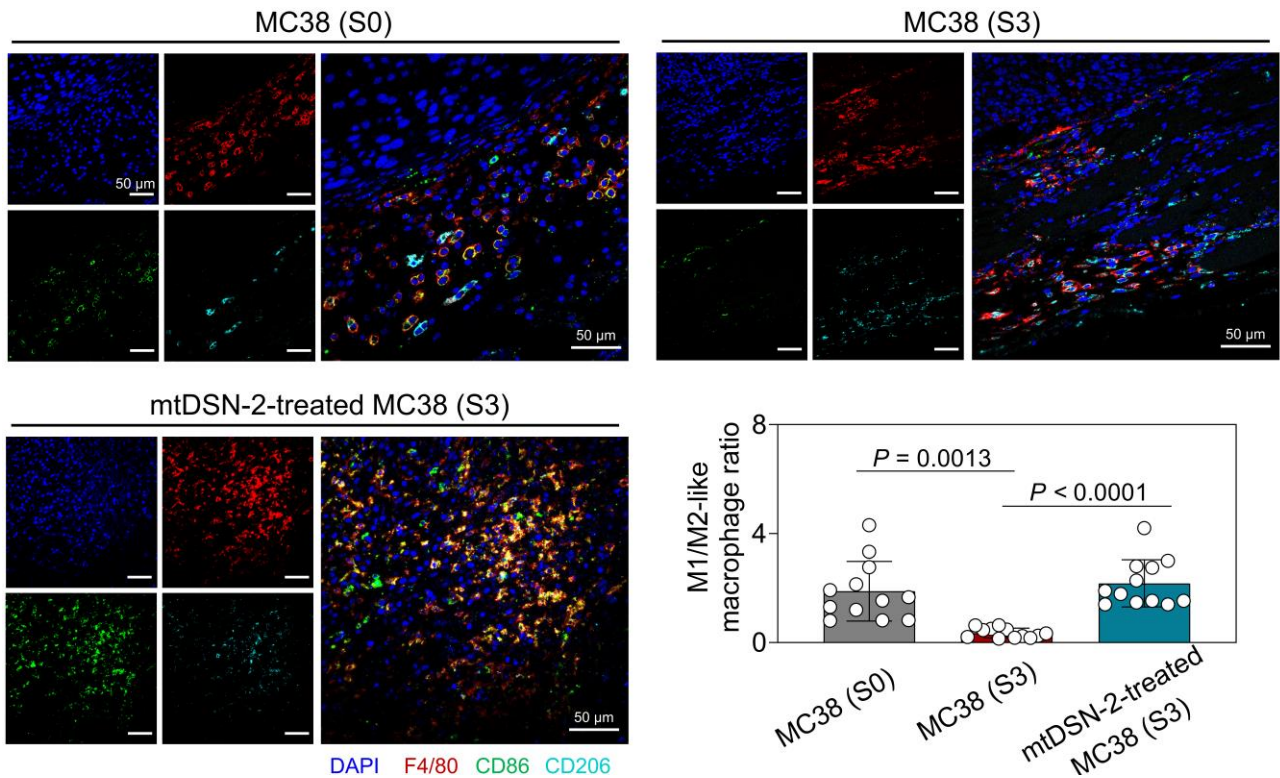
Supplementary Figure 24. Immunofluorescence observation and quantitative analysis of tumor-associated macrophages (TAMs) in S0, S3 and mtDSN-2 treated S3 tumors. M1-like macrophage, stained by F4/80 and CD86; M2-like macrophage, stained by F4/80 and CD206. The representative images and quantification of M1/M2-like macrophage ratio are shown from twelve different views of three independent samples. The data are presented as the mean ± s.d. Statistical analysis by Brown-Forsythe and Welch ANOVA with Dunnett's T3 multiple comparisons test. Source data are provided as a Source data file.
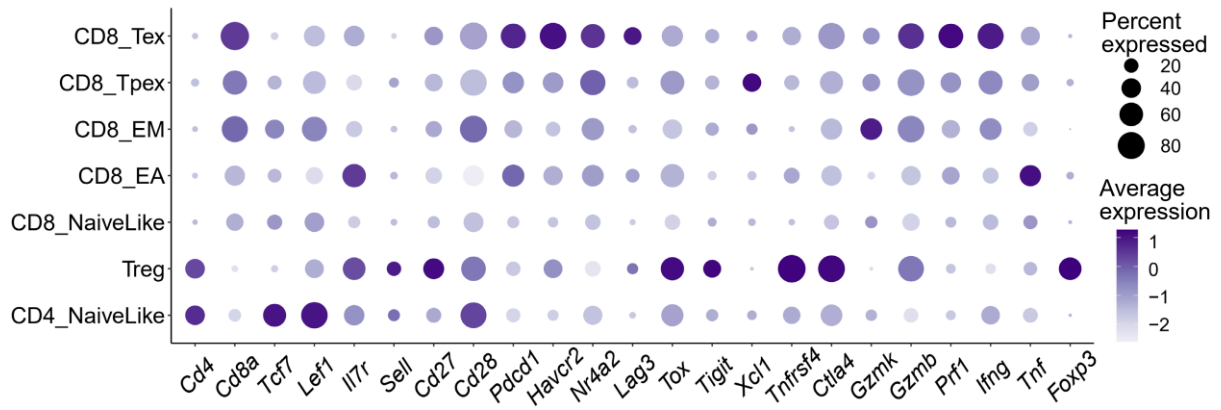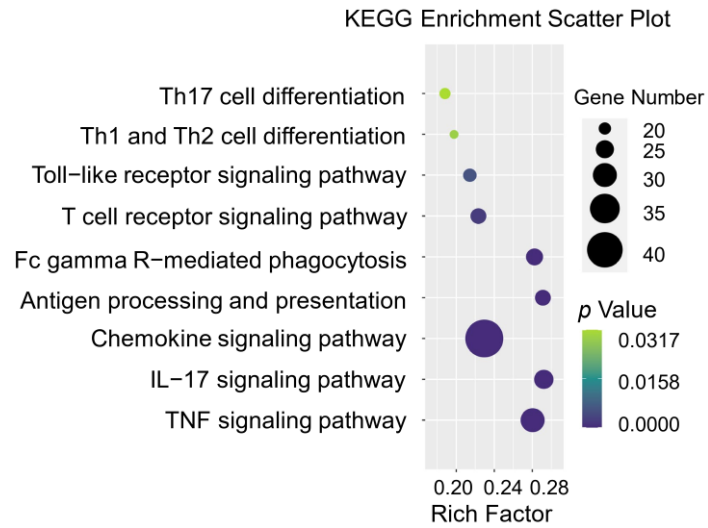
Supplementary Figure 25. T cells expressing indicated genes across subsets and their corresponding average expression (size of dot indicates the percentage of cells in each subset; expression intensity is indicated by color).
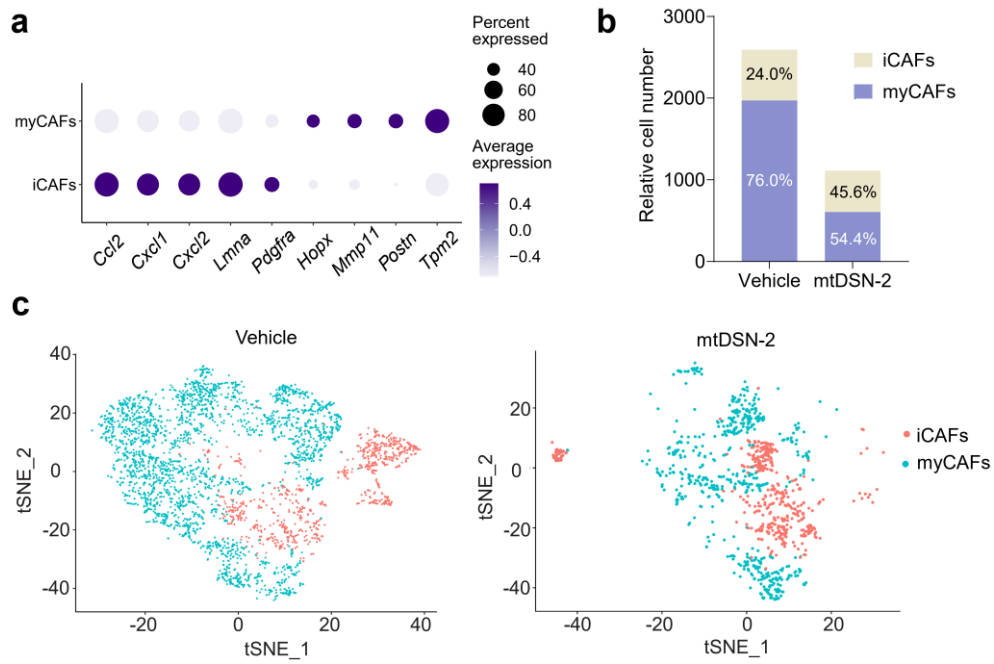
Supplementary Figure 26. a, Bubble plot outlining the expression of canonical lineage cell markers utilized for CAF cluster annotation. **b**, Stacked bar plot showing the proportion of the different cell clusters in CAFs. **c**, CAFs-only t-SNE projection showing emergent sub-clusters.
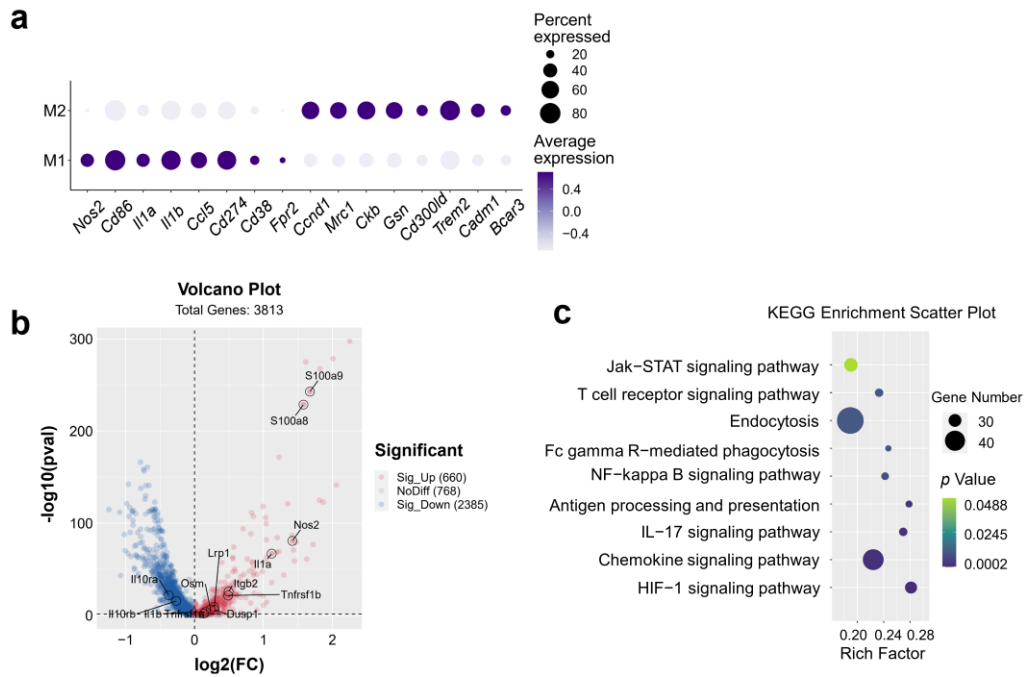
Supplementary Figure 27. a, Bubble plot outlining the expression of canonical lineage cell markers utilized for macrophage cluster annotation. **b**, Volcano plot showing changes in gene expression in the macrophage compartment of mtDSN-2 *vs.* vehicle treated tumors. Each dot represents one gene. The representative differential genes linked to the inflammasome pathway are labeled. **c**, KEGG analysis of DEGs showing pathways associated with antitumor response of macrophages after mtDSN-2 treatment.

Supplementary Figure 28. KEGG analysis of DEGs showing pathways associated with antitumor response of neutrophils after treatments.
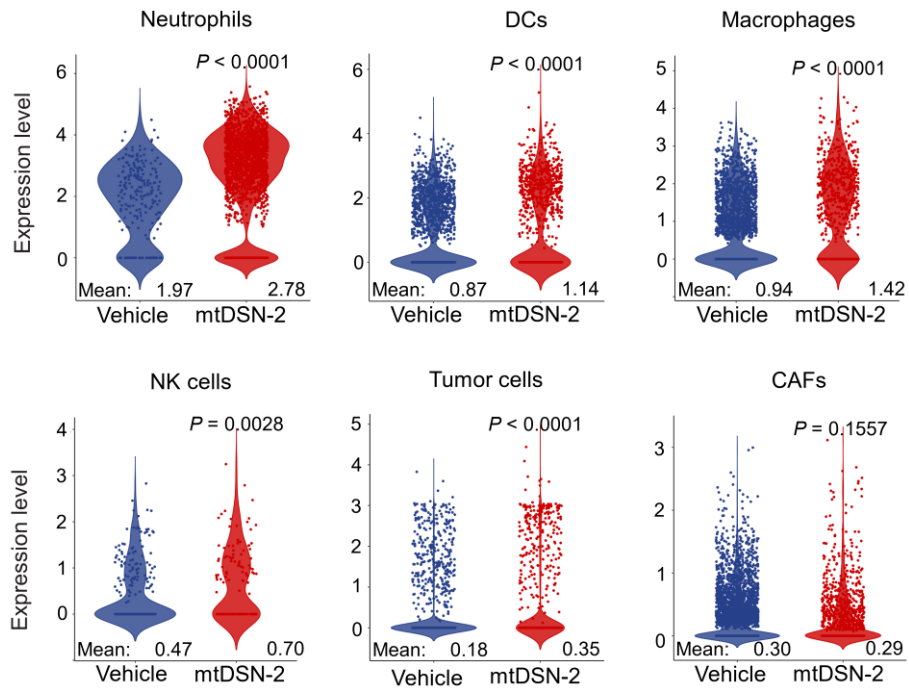
**Supplementary Figure 29.** Violin plots representing the expression of *CD274* (PD-L1) in different cell clusters after treatments. Statistical analysis by Wilcoxon rank sum test.
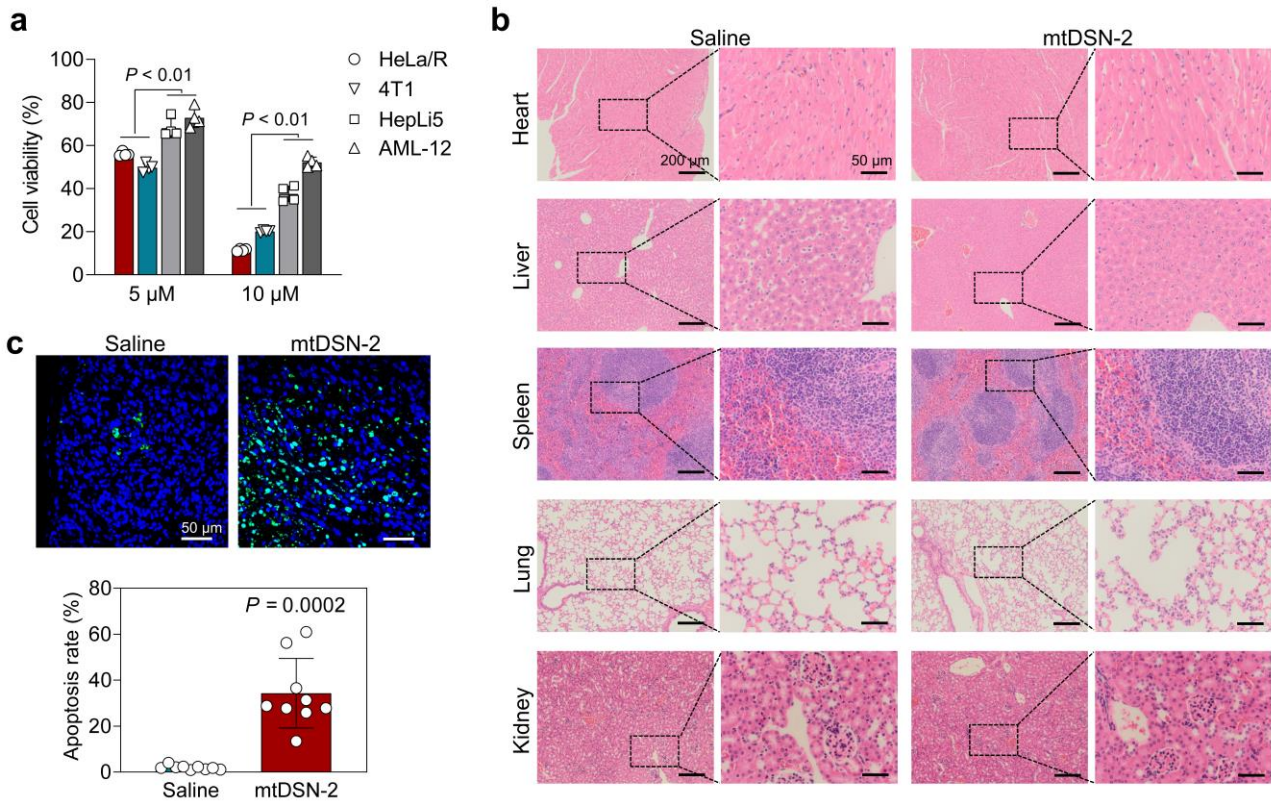
Supplementary Figure 30. a, Cytotoxicity of mtDSN-2 (5 μM or 10 μM for 48 h) in cancer cells (HeLa/R) and hepatocytes (AML12 and HepLi5) determined using MTT assay (n = 4). **b**, H&E staining of the major organs (n = 3 mice/group) after drug administration. **c**, Immunohistochemical analysis of the tumor apoptosis by TUNEL staining (n = 3 mice/group). The data are presented as the mean ± s.d. Statistical analysis by one-way ANOVA with Turkey's multiple comparisons test, Brown-Forsythe and Welch ANOVA with Dunnett's T3 multiple comparisons test (**a**) and Student's t test (**c**). Source data are provided as a Source data file.
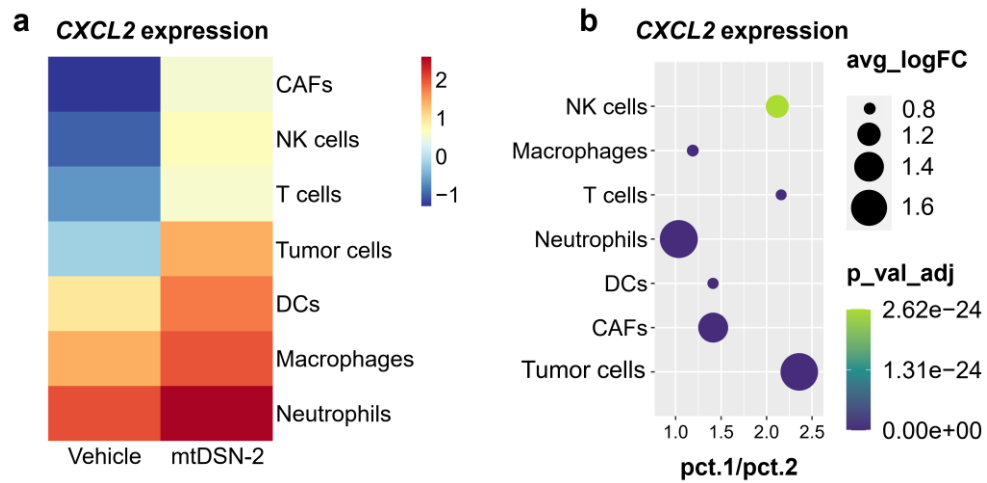
Supplementary Figure 31. a, Heat map of *CXCL2* expression among different cells. **b**, Scatter plot of *CXCL2* differential expression upon mtDSN-2 treatment relative to vehicle among different cells. pct.1/pct.2, the proportion of cells expressing *CXCL2* in mtDSN-2 group relative to that in vehicle group.
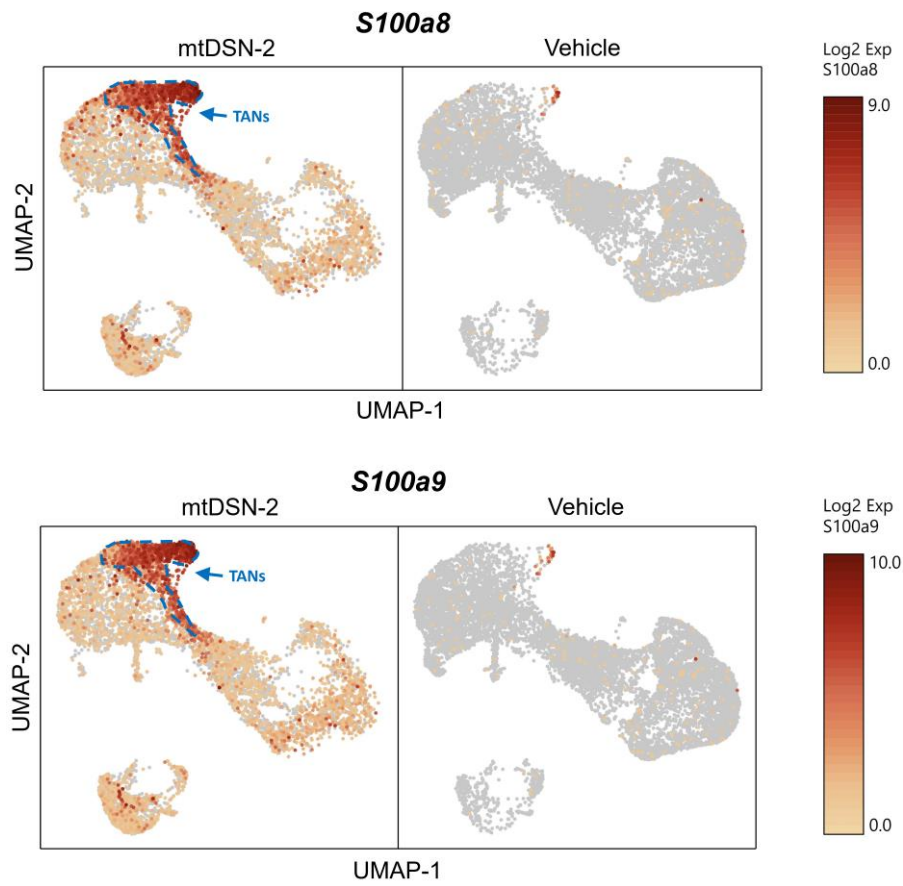
Supplementary Figure 32. Uniform manifold approximation and projection (UMAP) plots showing the expression level of *S100a8* and *S100a9* in the whole tumor. Blue dotted regions indicate the tumor-associated neutrophils (TANs).

	IC$_{50}$ (µM)					
Drug	HeLa	HeLa/R	A549	A549/R	A2780	A2780/R
Cisplatin	2.8 ± 0.1	10.1 ± 0.3	3.8 ± 0.6	16.6 ± 0.4	2.9 ± 0.3	13.8 ± 1.2
mtDSN-1	2.1 ± 0.2	3.6 ± 0.3	1.6 ± 0.1	1.9 ± 0.2	1.1 ± 0.1	1.3 ± 0.1
mtDSN-2	1.9 ± 0.2	3.0 ± 0.2	1.0 ± 0.1	1.7 ± 0.2	0.5 ± 0.04	1.2 ± 0.1
mtDSN-3	1.9 ± 0.2	3.4 ± 0.2	1.2 ± 0.1	2.0 ± 0.2	1.0 ± 0.1	1.3 ± 0.1
mtDSN-4	2.5 ± 0.2	4.0 ± 0.2	3.0 ± 0.2	2.4 ± 0.1	1.8 ± 0.1	2.1 ± 0.1
mtDSN-5	>100	>100	26.2 ± 4.0	34.8 ± 3.0	26.5 ± 2.6	29.3 ± 5.2

Supplementary Table 1. Cytotoxicity of cisplatin and mtDSN (IC$_{50}$, 72 h) against various cancerous cells (HeLa, A549, A2780) and their drug-resistance cell lines (HeLa/R, A549/R, A2780/R) determined by MTT assay (n = 3). All data are presented as the mean ± s.d.

	IC$_{50}$ (µM)					
Drug	HeLa	HeLa/R	A549	A549/R	A2780	A2780/R
TPP	>100	>100	>100	>100	69.0±4.5	>100
DHA	>100	>100	>100	>100	82.5±2.7	>100
LA	>100	>100	>100	>100	>100	>100
OA	>100	>100	>100	>100	>100	>100
Lau	>100	>100	>100	>100	>100	>100
Hep	>100	>100	>100	>100	>100	>100
TPP + DHA	82.0±10.8	>100	>100	>100	60.7±3.1	>100
TPP + LA	>100	>100	>100	>100	52.8±5.5	>100
TPP + OA	>100	>100	>100	>100	65.1±2.5	>100
TPP + Lau	>100	>100	>100	>100	62.1±3.3	>100
TPP + Hep	>100	>100	>100	>100	68.3±3.4	>100

Supplementary Table 2. Cytotoxicity of TPP or fatty acids alone and their combination (IC$_{50}$, 72 h) against various cancerous cells (HeLa, A549, A2780) and their drug-resistance cell lines (HeLa/R, A549/R, A2780/R) determined by MTT assay (n = 3). All data are presented as the mean ± s.d.